

Differential Rotation of Strong Magnetic Flux During Solar Cycles 21–23

W.B. Song · X.S. Feng · F. Shen · J.P. Guo

Received: 14 October 2010 / Accepted: 26 February 2011
© Springer Science+Business Media B.V. 2011

Abstract In the present investigation we measure the differential rotation of strong magnetic flux during solar cycles 21–23 with the method of wavelet transforms. We find that the cycle-averaged synodic rotation rate of strong magnetic flux can be written as $\omega = 13.47 - 2.58 \sin^2 \theta$ or $\omega = 13.45 - 2.06 \sin^2 \theta - 1.37 \sin^4 \theta$, where θ is the latitude. They agree well with the results derived from sunspots. A north–south asymmetry of the rotation rate is found at high latitudes ($28^\circ < \theta < 40^\circ$). The strong flux in the southern hemisphere rotates faster than that in the northern hemisphere by 0.2 deg day^{-1} . The asymmetry continued for cycles 21–23 and may be a secular property.

Keywords Magnetic fields · Rotation

1. Introduction

Solar differential rotation plays an important role in the construction of solar dynamos. Currently there are two basic methods of determining the rotation rate. One is to measure the positions of tracers on the surface or in the corona, and the other is to measure the line-of-sight velocities with the Doppler effect in spectrum lines (Howard, 1978). Sunspots are often used as tracers for their notability and long lifetime (see, *e.g.*, Balthasar and Wöhl, 1980; Howard, Gilman, and Gilman, 1984). Timothy, Krieger, and Vaiana (1975) analyzed an elongated coronal hole and found it to rotate with a synodic rate of $13.25 - 0.4 \sin^2 \theta \text{ deg day}^{-1}$, where θ is the latitude. (The synodic rotation rate is smaller than the sidereal rate by $360/365.25 \text{ deg day}^{-1}$.) There are many other visible features as tracers of solar rotation, such as Ca K faculae (Belvedere *et al.*, 1977) and quiescent filaments (Glackin, 1974). Snodgrass (1984) obtained a much smaller rate using the Dopplergrams. Pioneering work on the differential rotation of magnetic field patterns has been made by Wilcox and Howard (1970), Wilcox *et al.* (1970), and Stenflo (1974). Knaack, Stenflo, and Berdyugina (2005) analyzed

W.B. Song (✉) · X.S. Feng · F. Shen · J.P. Guo
SIGMA Weather Group, State Key Laboratory of Space Weather, Center for Space Science and Applied Research, Chinese Academy of Sciences, Beijing 100190, China
e-mail: wbsong@spaceweather.ac.cn

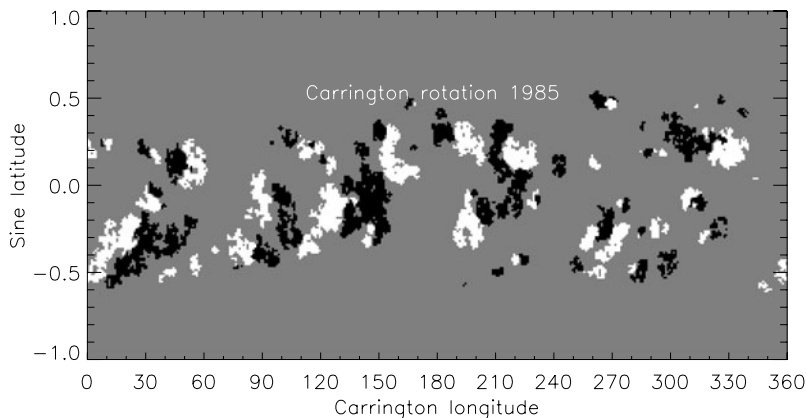


Figure 1 Strong magnetic flux of CR 1985. Here we follow the selection criterion given by Song *et al.* (2009).

the rotation of large-scale photospheric magnetic fields in each solar hemisphere. Although great effort has been invested in the past, the picture that has emerged is confusing since various methods give different results (Stenflo, 1989). Based on the classification of solar global magnetic flux proposed by Song *et al.* (2009), using magnetic synoptic charts we measure the rotation rate of the strong flux which mostly comes from active regions. Compared to the rotation rate of sunspots, the rotation rate of active regions (more fundamental structures than sunspots) has not drawn attention very much so far. This is partly because there may be an ambiguity in defining the extent of active regions on the Sun.

2. Data and Method

Solar magnetic synoptic charts can be used to explore the rotation rate mostly due to the long lifetime of strong magnetic flux (see, *e.g.*, Wilcox and Howard, 1970; Stenflo, 1974). Such tracers are quite similar to the recurrent sunspots studied by Newton and Nunn (1951). In this investigation, the data we employed are Carrington-coordinate magnetic synoptic charts produced by NSO/Kitt Peak during Carrington rotation (CR) 1625–2007, and by SOHO/MDI during CR 2008–2092. Song *et al.* (2009) proposed a selection criterion for strong magnetic components: in a global grid of 360 equal steps in longitude by 180 equal steps in sine latitude, for any pixel to belong to strong magnetic components, the mean flux density of its nearest 1, 5, 13, 29, and 49 pixels (including itself) should be all greater than 25 gauss. Following this criterion we exclude the dispersed magnetic pieces related to extended bipolar regions (EBRs) and weak magnetic components from the synoptic charts, as shown in Figure 1. It depicts the global distribution of strong magnetic flux of CR 1985 with a grid of 360 equal steps in longitude by 180 equal steps ($i = 0, 1, 2, \dots, 179$, marked from the south pole to the north pole) in sine latitude.

As a result, we find that the area covered with strong magnetic flux during solar minima is very small at high latitudes. Moreover, the lifetime of most of them is less than one rotation. In the above situation it is very difficult to calculate the rotation rate accurately. Thus we only study the rotation of the strong flux located at middle latitudinal strips (here $i = 30 - 149$ or $|\theta| \leq 41.4^\circ$, $\theta = \frac{180}{\pi} \times \arcsin \frac{i-89.5}{90}$; see Figure 2(a)) and during the time intervals excluding the activity minima (CR 1660–1750, CR 1800–1880, and CR 1925–2025, as shown in

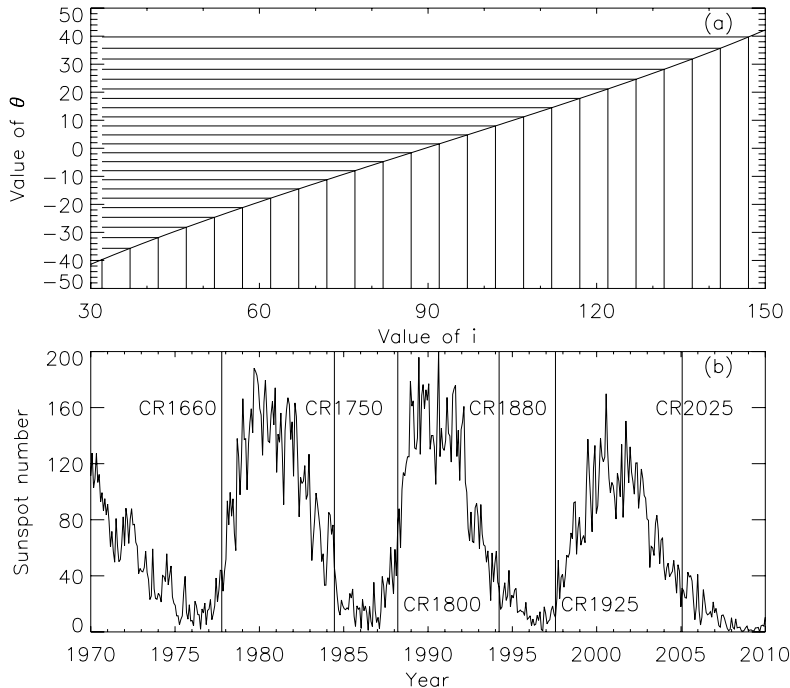


Figure 2 (a) The latitude θ corresponding to the value of i . 24 vertical lines are located where $i = 32, 37, 42, \dots, 147$; (b) The monthly sunspot number. Vertical lines mark the three time intervals we selected.

Figure 2(b)). Figure 3 gives an example. First we re-arrange and connect the magnetic charts in a time series (Stenflo and Güdel, 1988) and obtain a long chart. Then we separate the mid-latitude part of this long chart into 24 strips: each strip represents five steps in sine latitude, such as $i = 30 - 34$, $i = 35 - 39$, etc. We assume that the meridional motions of magnetic flux can be ignored (Howard and Gilman, 1986), which ensures us of the reliability of studying each latitudinal strip. Secondly for anyone strip, we add the number of non-zero pixels (in proportion to the area of strong magnetic flux) at every longitudinal step. Figure 3(a) is for the strip of $i = 120 - 124$ during CR 1660 – 1750. Figure 3(b) is an enlargement of the red part of the sequence in Figure 3(a). From it we find that the peaks originating from the same active regions (e.g., green and blue ones) are located at similar Carrington longitudes (CL). The continuous emergence of recurrent magnetic structures makes all the time sequences constructed above contain a very distinct rotation period. Assuming the length of the rotation period is p measured in the unit of 1 CL = 27.275/360 day (27.275 day is the synodic Carrington rotation period), the synodic rotation rate ω in deg day $^{-1}$ should be

$$\omega = \frac{360}{p \times 27.275/360} = \frac{4751.6}{p}. \quad (1)$$

Typical methods for finding periodicity include the fast Fourier transform (FFT), the Scargle periodogram (Scargle, 1982), and the wavelet transform (WT). Since FFT and Scargle power densities are not smooth functions of the period, it is difficult to determine the value of p convincingly. Therefore, we choose the WT method in which a Morlet wavelet

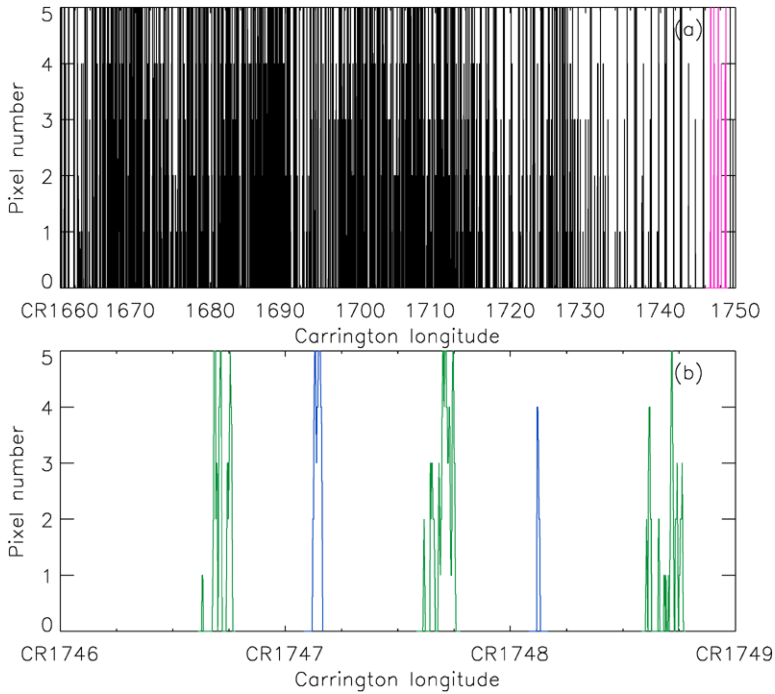


Figure 3 (a) The area of strong magnetic flux in region of sine latitudinal steps $i = 120\text{--}124$ ($19.8^\circ < \theta < 22.5^\circ$) during CR 1660–1750. The size of single pixel is $4\pi R_\odot^2/(360 \times 180)$. (b) Enlargement of the red part of the sequence in (a). The peaks of different colors originate from different active regions.

is used as the base function. The Morlet wavelet function is initially proposed by Morlet *et al.* (1982) and later reintroduced by Daubechies (1992). It has turned out to be well adapted to analyzing the time sequences. The expression of a Morlet wavelet is a plane cosine wave modulated by a Gaussian function, $\Psi(x) = e^{-x^2/2} \cos(kx)$. Because the Fourier transform of a Gaussian function is itself a Gaussian, the Morlet WT can be fine-tuned to have good resolutions in both time and frequency domains. We choose $k = 6$ in order to make $\Psi(x)$ to satisfy the condition of $\int_{-\infty}^{+\infty} \Psi(x) dx = 0$ approximately and to guarantee a good correspondence between the Fourier period (n) and the Morlet wavelet time scale (s). Here n and s are related by $n = 4\pi s/(k + \sqrt{2 + k^2})$. When $k = 6$ we obtain $n = 1.03s$. For a signal $f(n)$, its WT spectrum is defined as

$$W(n, s) = |s|^{-1/2} \int_{-\infty}^{+\infty} f(n) \overline{\Psi\left(\frac{n-t}{s}\right)} dt. \quad (2)$$

This definition tells us that WT can yield periodicity information in time and frequency domains simultaneously, since its base function is band-limited. The global wavelet power density is defined by

$$M(s) = \int |W(n, s)|^2 dn, \quad (3)$$

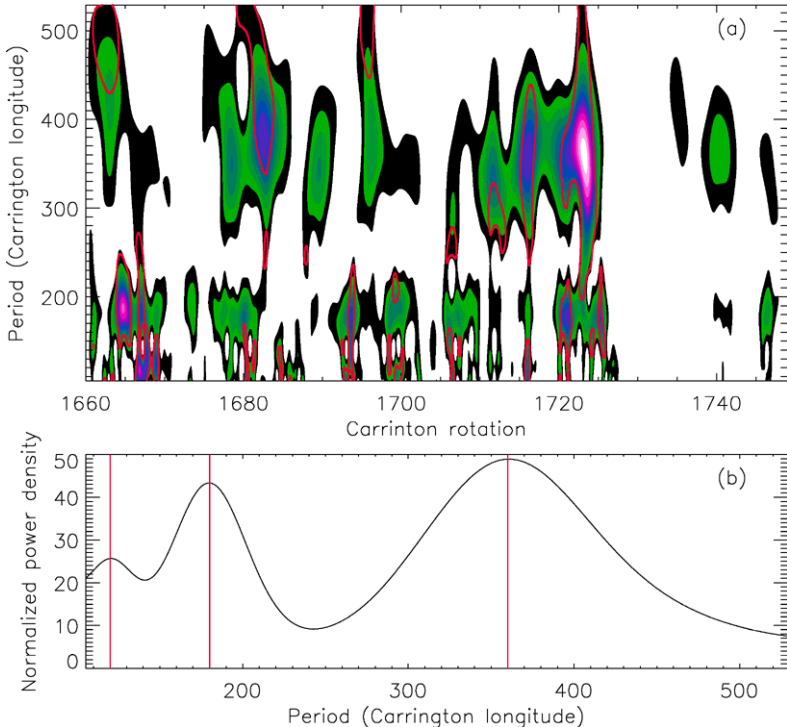


Figure 4 (a) Period-time contour of the wavelet power density of the sequence of $i = 120\text{--}124$ ($19.8^\circ < \theta < 22.5^\circ$) during CR 1660–1750. The red curves indicate the 95% significance level. (b) The normalized global wavelet power density. Three distinct peaks can be found. They are the rotation period and its two harmonics.

which shows the average periodicity during the whole time interval. The significance level of peaks in a WT spectrum can be derived from a null hypothesis by assuming that the noise is distributed independently on the periods (Torrence and Compo, 1998).

3. Results and Discussion

Figure 4(a) shows the period-time contour of the wavelet power density of the sequence of $i = 120\text{--}124$ ($19.8^\circ < \theta < 22.5^\circ$) during CR 1660–1750 (solar cycle 21). From it we find that the rotation period near 360 CL fluctuates most clearly. The variabilities in the rotation period and its component amplitude mainly come from continuous evolution of recurrent strong magnetic flux. Balthasar, Vázquez, and Wöhl (1986) have found a very slow deceleration in recurrent sunspot groups. However, we pay more attention to the cycle-averaged rotation rate in the present study. Figure 4(b) shows the global wavelet power density which represents the average periodicity during the whole time interval. The power density shows a very smooth variation with three distinct peaks located at 360, 180, and 120 CLs, respectively. Even a single strong magnetic flux structure may evolve significantly in one CR, and the change in its center position can affect the measurement of its rotation period. Because there exist many such structures in the whole time interval, their random evolution gives a considerable width to the rotation period (e.g. the component near the

Table 1 The lengths of the rotation period (T_1) and its two harmonics (T_2 and T_3) for three solar cycles (SC 21–23). The unit of period is 1 CL = 27.275/360 day. The asterisk means that the period is not distinct.

Value of i	SC 21			SC 22			SC 23		
	T_1	T_2	T_3	T_1	T_2	T_3	T_1	T_2	T_3
30–34	388	186	129	376	194	126	374	190	*
35–39	396	186	125	384	188	125	367	186	124
40–44	372	182	124	370	188	123	362	185	123
45–49	366	181	124	357	187	121	365	184	121
50–54	356	180	123	352	184	119	364	183	120
55–59	364	180	*	345	184	119	361	182	122
60–64	370	179	119	344	181	120	352	181	*
65–69	365	179	118	356	180	120	350	180	*
70–74	364	178	120	361	181	*	356	178	119
75–79	364	179	118	361	180	117	353	177	119
80–84	364	177	117	364	176	119	350	177	118
85–89	355	175	118	328	177	119	356	181	112
90–94	349	175	*	345	180	118	357	175	*
95–99	348	177	118	356	181	120	348	173	117
100–104	355	178	117	357	179	119	348	179	117
105–109	358	178	118	359	178	120	351	179	118
110–114	359	177	119	360	177	119	351	178	119
115–119	362	177	120	365	179	119	349	178	119
120–124	360	180	120	367	178	121	348	182	120
125–129	358	184	120	368	179	125	348	184	122
130–134	380	183	123	376	187	123	370	186	123
135–139	395	190	124	373	187	124	379	189	125
140–144	392	193	130	380	189	126	374	190	124
145–149	384	193	*	394	189	130	374	194	130

period of 360 CL in Figure 4(b)). In order to obtain a more realistic value of p , we also consider the other two shorter periods found at 120 and 180 CLs. As given in Table 1, we find one or two such similar periods in all 72 time sequences. Their periods are always close to one half or one third of those of their corresponding rotation periods. We think that they are the second and third harmonics of the rotation period. Song and Wang (2005) even found the eighth harmonic in the FFT power spectrum. The appearance of harmonics could be due to some non-sinusoidal inputs like the periodic pulse signals, *e.g.*, the green and blue peaks in Figure 3(b). On considering two harmonics, we give a new value to p as follows

$$p = (p_1 + p_2 \times 2 + p_3 \times 3)/3, \quad (4)$$

where p_1 , p_2 , and p_3 are the peak positions of solar rotation and its two harmonics. If the third harmonic is not distinct (see the asterisks in Table 1), then Equation (4) should be changed to

$$p = (p_1 + p_2 \times 2)/2. \quad (5)$$

Then, by using Equation (1), the rotation rate can be calculated.

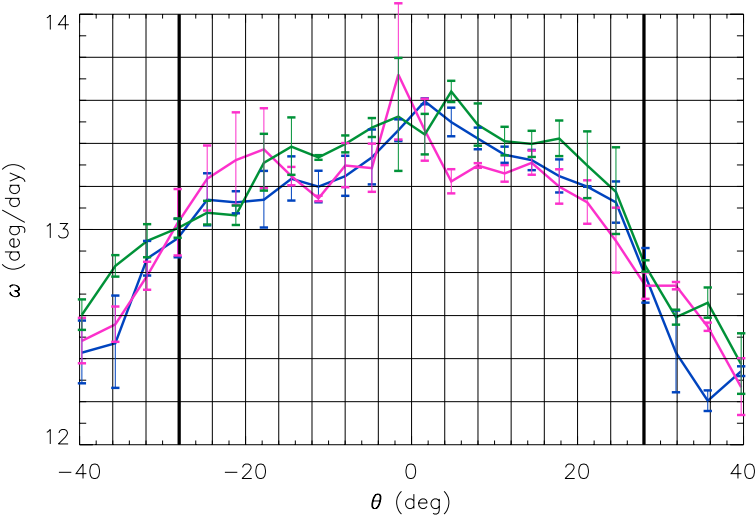


Figure 5 The rotation rate of strong magnetic flux (blue: solar cycle 21; red: solar cycle 22; green: solar cycle 23). Two black vertical lines are located at $\theta = \pm 28.2^\circ$.

Three curves in Figure 5 show the results of solar cycles 21 (blue), 22 (red), and 23 (green). The differential rotation is clear – the rotation rates decrease from the equator to higher latitudes. These curves entangle with each other and do not exhibit obvious differences among them. In other words, the cycle-averaged rotation rate is quite steady. Therefore we perform a least-square fit of the function $\omega = a + b \sin^2 \theta$ for three solar cycles simultaneously. Each latitudinal strip is represented by the central value of i , namely, for the strip of $i = 75 - 79$, we choose $\theta = \frac{180}{\pi} \times \arcsin \frac{77-89.5}{90} = -8.0^\circ$. The latitudes of all strips are marked by 24 vertical lines in Figure 2(a). We have obtained $a = 13.47(\pm 0.04)$ and $b = -2.58(\pm 0.18)$ deg day $^{-1}$. It agrees well with the results derived by Newton and Nunn (1951) using the recurrent sunspots and by Lustig (1983) using sunspot data during years 1947–1981. This is easy to understand because sunspots belong to strong magnetic flux regions. Stenflo (1974) obtained a slightly faster rotation rate in the longitudinal magnetic field patterns. To make a comparison with the rotation of small magnetic features (Komm, Howard, and Harvey, 1993a, 1993b), we performed a least-square fit of another function $\omega = a + b \sin^2 \theta + c \sin^4 \theta$ and have obtained $a = 13.45(\pm 0.04)$, $b = -2.06(\pm 0.31)$, and $c = -1.37(\pm 0.80)$ deg day $^{-1}$. The values of a and b are in good agreement with their results. However, our value of c is larger by 0.72 deg day $^{-1}$.

Lustig (1983) found that the southern hemisphere has a smaller gradient (a smaller value of $|b|$) of the differential rotation than the northern hemisphere does. This means that the southern hemisphere rotates faster than the northern hemisphere. He argued that such asymmetry is a peculiar behavior of the period 1947–1981. From Figure 5 we find a different rotation rate mainly occurs at high latitudes (beyond two thick vertical lines where $\theta \geq 28.2^\circ$). The southern hemisphere rotates faster roughly by 0.2 deg day $^{-1}$. In the study of Chu *et al.* (2010), they did not find this phenomenon, possibly because their magnetic flux data also included EBRs. EBRs show significant diffusion and may have affected the measurement of rotation rate. To further test this north–south asymmetry of the rotation rate at high latitudes, we have added up time sequences of $i = 30 - 34, 35 - 39, 40 - 44, 45 - 49$ for the southern hemisphere and of $i = 130 - 134, 135 - 139, 140 - 144, 145 - 149$ for the northern

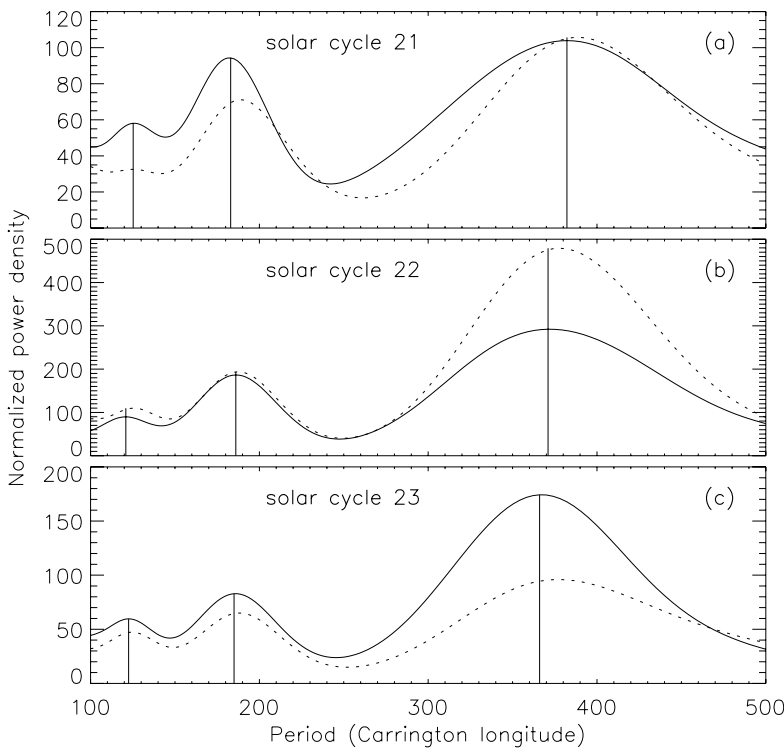


Figure 6 The normalized global wavelet power density of strong magnetic flux at high latitudes. The solid lines are for the southern hemisphere with $i = 30-49$ or $-39.7^\circ < \theta < -28.2^\circ$, and the dashed lines are for the northern hemisphere with $i = 130-149$ or $28.2^\circ < \theta < 39.7^\circ$.

hemisphere, and then calculate global WT power spectra of these sequences (Figure 6). From this figure we find that the rotation period and its two harmonics of the southern hemisphere are all shorter than those of the northern hemisphere during each solar cycle. Thus we believe that a faster rotation rate found in the southern high latitudes is real.

4. Conclusions

Following the selection criterion proposed by Song *et al.* (2009), we have selected the pure strong magnetic flux from 468 synoptic charts. Seventy-two time sequences of the area of strong flux between latitudes $\pm 39.7^\circ$ and during solar cycles 21–23 were constructed. Since the plot of global wavelet power density is much smoother than other typical power spectra, *e.g.*, FFT and Scargle spectra, we have used it to find the rotation period in the above sequences. As a result, three distinct periods were found: one is the rotation period, and the other two are its harmonics. From the values of such three periods, we investigated the differential rotation rates in detail. We found that the synodic rotation rate of strong magnetic flux is represented by $\omega = 13.47 - 2.58 \sin^2 \theta$ or $\omega = 13.45 - 2.06 \sin^2 \theta - 1.37 \sin^4 \theta$, which is in agreement with the results derived from sunspots. There exists a north–south asymmetry of the rotation rate at high latitudes ($28^\circ < \theta < 40^\circ$). The strong flux in the southern hemisphere rotates faster by 0.2 deg day^{-1} than that in the northern hemisphere.

However, to further examine where this difference comes from is beyond the scope of our present study.

Acknowledgements The wavelet software was provided by C. Torrence and G. Compo. It is available at URL: <http://paos.colorado.edu/research/wavelets/>. This work is jointly supported by the National Natural Science Foundation of China (Grant Nos. 40921063, 40974107, 40890161, 41031066, 40874091, and 41074122), and the Specialized Research Fund for State Key Laboratories.

References

- Balthasar, H., Wöhl, H.: 1980, *Astron. Astrophys.* **92**, 111.
Balthasar, H., Vázquez, M., Wöhl, H.: 1986, *Astron. Astrophys.* **155**, 87.
Belvedere, G., Godoli, G., Motta, S., Paternò, L., Zappalà, R.: 1977, *Astrophys. J. Lett.* **214**, 91.
Chu, Z., Zhang, J., Nie, Q., Li, T.: 2010, *Solar Phys.* **264**, 1.
Daubechies, I.: 1992, *Ten Lectures on Wavelets*, Society for Industrial and Applied Mathematics, Philadelphia.
Glackin, D.: 1974, *Solar Phys.* **36**, 51.
Howard, R.: 1978, *Rev. Geophys. Space Phys.* **16**, 721.
Howard, R., Gilman, P.A.: 1986, *Astrophys. J.* **307**, 389.
Howard, R., Gilman, P.A., Gilman, P.I.: 1984, *Astrophys. J.* **283**, 373.
Knaack, R., Stenflo, J., Berdyugina, S.: 2005, *Astron. Astrophys.* **438**, 1067.
Komm, R., Howard, R., Harvey, J.: 1993a, *Solar Phys.* **143**, 19.
Komm, R., Howard, R., Harvey, J.: 1993b, *Solar Phys.* **145**, 1.
Lustig, G.: 1983, *Astron. Astrophys.* **125**, 355.
Morlet, J., Arens, G., Forgeau, I., Giard, D.: 1982, *Geophysics* **47**, 203.
Newton, H., Nunn, M.: 1951, *Mon. Not. Roy. Astron. Soc.* **111**, 413.
Scargle, J.: 1982, *Astrophys. J.* **263**, 835.
Snodgrass, H.: 1984, *Solar Phys.* **94**, 13.
Song, W., Wang, J.: 2005, *Astrophys. J. Lett.* **624**, 137.
Song, W., Feng, X., Shen, F., Zhang, Y.: 2009, *Solar Phys.* **257**, 83.
Stenflo, J.: 1974, *Solar Phys.* **36**, 495.
Stenflo, J.: 1989, *Astron. Astrophys.* **210**, 403.
Stenflo, J., Güdel, M.: 1988, *Astron. Astrophys.* **191**, 137.
Timothy, A., Krieger, A., Vaiana, G.: 1975, *Solar Phys.* **42**, 135.
Torrence, C., Compo, G.: 1998, *Bull. Am. Meteorol. Soc.* **79**, 61.
Wilcox, J., Howard, R.: 1970, *Solar Phys.* **13**, 251.
Wilcox, J., Schatten, K., Tanenbaum, A., Howard, R.: 1970, *Solar Phys.* **14**, 255.